AJNR

Diffusion-Weighted Imaging in the Follow-up of Treated High-Grade Gliomas: Tumor Recurrence versus Radiation Injury

Patrick A. Hein, Clifford J. Eskey, Jeffrey F. Dunn and Eugen B. Hug

AJNR Am J Neuroradiol 2004, 25 (2) 201-209
http://www.ajnr.org/content/25/2/201

AJNR Am J Neuroradiol 25:201–209, February 2004

Diffusion-Weighted Imaging in the Follow-up of Treated High-Grade Gliomas: Tumor Recurrence versus Radiation Injury

Patrick A. Hein, Clifford J. Eskey, Jeffrey F. Dunn, and Eugen B. Hug

BACKGROUND AND PURPOSE: **Diffusion-weighted (DW) MR imaging is a means to characterize and differentiate morphologic features, including edema, necrosis, and tumor tissue, by measuring differences in apparent diffusion coefficient (ADC). We hypothesized that DW imaging has the potential to differentiate recurrent or progressive tumor growth from treatment-induced damage to brain parenchyma in high-grade gliomas after radiation therapy.**

METHODS: **We retrospectively reviewed follow-up conventional and DW MR images obtained starting 1 month after completion of radiation treatment with or without chemotherapy for histologically proved high-grade gliomas. Eighteen patients with areas of abnormal enhancing tissue were identified. ADC maps were calculated from echo-planar DW images, and mean ADC values and ADC ratios (ADC of enhancing lesion to ADC of contralateral white matter) were compared with final diagnosis. Recurrence was established by histologic examination or by clinical course and a combination of imaging studies.**

RESULTS: **Recurrence and nonrecurrence could be differentiated by using mean ADC values and ADC ratios. ADC ratios in the recurrence group showed significantly lower values (mean ± SD, 1.43 ± 0.11) than those of the nonrecurrence group (1.82 ± 0.07, $P < .001$). Mean ADCs of the recurrent tumors (mean ± SD, 1.18 ± 0.13 × 10^{-3} mm/s^2) were significantly lower than those of the nonrecurrence group (1.40 ± 0.17 × 10^{-3} mm/s^2, $P < .006$).**

CONCLUSION: **Assessment of ADC ratios of enhancing regions in the follow-up of treated high-grade gliomas is useful in differentiating radiation effects from tumor recurrence or progression.**

The radiologic differentiation of treatment effects from recurrent or progressing neoplasm after radiation therapy and chemotherapy for high-grade gliomas is difficult. Modalities used to assess abnormal lesions in the follow-up of treated malignant brain tumors include CT, conventional and perfusion MR imaging, MR spectroscopy, positron emission tomography (PET), and single photon emission CT (SPECT) (1–4). Most such lesions, usually represented by a contrast material–enhancing mass with surrounding edema, are located in or near the primary site of disease and within the irradiated volume (5). Both recurrent neoplasms and therapy-induced lesions have a similar radiologic appearance owing to alterations of the blood-brain barrier.

Received June 16, 2003; accepted after revision August 21.

From the Section of Radiation Oncology, Norris Cotton Cancer Center (P.A.H., E.B.H.) and the Department of Radiology (C.J.E., J.F.D.), Dartmouth-Hitchcock Medical Center, Lebanon, NH.

Address reprint requests to Patrick A. Hein, MD, Department of Radiology, Charité, Humboldt Universitaet zu Berlin, Schumannstr. 20/21, 10098 Berlin, Germany.

Diffusion-weighted (DW) imaging has been considered a means to characterize and differentiate morphologic features, including edema, necrosis, and tumor tissue, by measuring differences in apparent diffusion coefficient (ADC) caused by water proton mobility alterations (6, 7). These differences are thought to result from both changes in the balance between intracellular and extracellular water and changes in the structure of the two compartments. Previous neuro-oncologic studies applied this technique to evaluate cellularity in gliomas, to determine tumor grade noninvasively (8). Signal intensity and ADCs in neoplastic tissue, peritumoral edema, and normal brain tissue have been reported for low- and high-grade gliomas, meningiomas, and brain metastases (9). Necrotic brain tissue in the temporal lobe after radiation therapy of nasopharyngeal carcinoma has been characterized with DW imaging (10). Previously reported ADC values for high-grade glial neoplasms vary from 1.1 to 1.37 × 10^{-3} mm/s^2 (8, 11, 12). ADCs in peritumoral edema or temporal lobe necrosis after radiation therapy of nasopharyngeal carcinomas were reported as 1.29 and 2.88 × 10^{-3} mm/s^2 in two studies, respectively (7, 10).

There are clear histologic differences between recurrent neoplasm and brain parenchyma altered by aggressive treatment. High-grade glial neoplasms are represented by areas of viable cells with pleomorphic nuclei and a dense network of cytoplasmic processes, whereas posttreatment necrosis shows only a paucity of viable cells. We hypothesized that ADC values and ADC ratios in contrast-enhancing areas after treatment for high-grade glioma would be lower in recurrent neoplasm than in treatment-induced necrosis.

Methods

Patients

Images for this retrospective study were selected from all cases of patients treated for high-grade (World Health Organization [WHO] grade III or IV) glial neoplasms at our hospital in 2001 and 2002. All of the patients had undergone surgical resection or stereotactic biopsy of the tumor at the time of diagnosis and subsequently a full course of fractionated, 3D-conformal radiation therapy.

Medical records were reviewed for posttreatment follow-up MR images on which new enhancing regions were identified. Twenty-two patients initially met this criterion. Excluded were two patients whose follow-up imaging was not performed or continued at our institution (ie, available diagnostics were not sufficient to reveal final diagnosis). Another two patients were excluded because the area of new enhancement was not sufficiently large to be accurately identified on generated ADC maps.

The images of 18 patients were included for final analysis (13 male and five female patients; mean age, 52 years; age range, 14–77 years). Histologic diagnosis of the primary site in these cases was as follows: glioblastoma multiforme WHO grade IV, eight patients; anaplastic astrocytoma WHO grade III, three patients; anaplastic oligodendroglioma WHO grade III, two patients; and anaplastic mixed glioma WHO grade III, five patients. Initial tumor diagnosis, treatment parameters, and imaging modalities are summarized in Table 1. The reader is referred to the Journal's Web site (www.ajnr.org) to obtain information provided in Table 1 about patient, tumor, and treatment characteristics; radiologic diagnostic modalities, including diagnosis of the primary neoplasm; and radiation doses and chemotherapeutic agents used in each patient.

Patients were grouped according to MR enhancement that was due either to tumor recurrence (recurrence group, n = 12) or to treatment-induced necrosis (nonrecurrence group, n = 6). In seven of the 18 cases, final diagnosis was confirmed histologically by means of biopsy or resection of the newly enhancing area. In 11 cases, group allocation was based on a combination of clinical course and repeat combined radiologic imaging (MR imaging, MR spectroscopy, PET, and SPECT), and on consensus of the multidisciplinary neuro-oncology team. Table 2 on the Journal's Web site contains further information about time to MR imaging enhancement after completion of radiation therapy, subsequent clinical course, and radiographic development. In 14 of 18 cases, diagnoses were available before this study was started. Four patients who met the inclusion criteria of initial high-grade tumor diagnosis and specific radiographic appearance were analyzed prospectively and included after the group allocation was established. In all patients in the nonrecurrence group, the clinical symptoms stabilized during the time of follow-up after newly diagnosed MR enhancement. However, all seven patients in the recurrence group who did not have histologic confirmation experienced progressive functional deterioration and failure of steroid therapy consistent with progressive disease.

Tumor recurrence was radiologically defined as steady growth of enhancement and mass effect despite steroid therapy. In case of incomplete resection, tumor progression was defined as marked enlargement of the residual, enhancing region within the tumor and as progressive enlargement on follow-up studies. Nonrecurrence was radiologically defined as stable-appearing or resolving regions of enhancement. In nine patients, a combination of different imaging modalities, including fluorine-18-deoxyglucose (FDG) PET, thallium-201 SPECT, and single or multivoxel proton MR spectroscopy, were used to make the diagnosis. For PET, the presence of recurrent neoplasm was determined from qualitative presence of abnormal increased uptake at the tumor bed; absence of such increased uptake was considered as treatment-induced necrosis. For ^{201}Tl SPECT, the presence of recurrent neoplasm was determined from qualitative presence of abnormal increased uptake at the tumor bed; absence of such increased uptake was considered as treatment-induced necrosis. For proton MR spectroscopy, the presence of recurrent neoplasm was determined from the presence of an area with a choline-to-creatine ratio greater than 3:1; lower values were considered indeterminate. All determinations were made by board-certified radiologists or nuclear medicine physicians as part of the clinical care of the patients. If the final diagnosis was solely defined by the radiologic appearance on follow-up standard MR images, further follow-up had to exceed 4 months or consist of at least three follow-up imaging studies. Patients in the recurrence group who died from their cerebral disease were excepted from this limit.

Treatment

After tumor resection or biopsy, all patients underwent a full course of fractionated, 3D-conformal radiation therapy. Patients were treated to total doses between 57.6 and 66.6 Gy, at 1.8–2-Gy dose per fraction. Megavoltage photon radiation was provided by a linear accelerator and applied in multiple field arrangements as per 3D treatment plan. The duration of treatment was between 6 and 7 weeks (30–37 fractions), depending on the dose per fraction. Patients with glioblastoma multiforme received 60–66.6 Gy, and patients with glioma grade III received 57.6–66.6 Gy. Twelve of 18 patients received an additional chemotherapeutic regimen: five patients with glioblastoma multiforme and seven patients with anaplastic glioma. Chemotherapeutic regimens included the following agents: chloroethylcyclohexylnitrosourea ([CCNU] lomustine); camptothecin-11 (irinotecan); temozolomide (Temodar); and procarbacin, CCNU, vincristin (PCV).

MR Acquisition

Follow-up imaging started in the first month after completed radiation therapy and was repeated in intervals between 1 and 3 months, depending on the clinical course. MR examinations were performed with a 1.5-T imaging system (GE Medical Systems, Milwaukee, WI). Patients scheduled for imaging were assigned to the specific MR imaging protocol for brain neoplasms at our institution. This protocol consisted of axial precontrast and triplanar postcontrast T1-weighted imaging (400/14/1.5 [TR/TE/excitations], field of view 20 × 20 cm, acquisition matrix 256 × 192 pixels, 6-mm section thickness with 3-mm gap), axial fast spin-echo T2-weighted imaging (3500/104/2, echo train length 8–12, field of view 20 cm, acquisition matrix 256 × 192 pixels, 6-mm section thickness with 3-mm gap), axial fluid-attenuated inversion-recovery (FLAIR) imaging (10,002/175/2200/1 [TR/TE/TI/excitation], field of view 20 cm, acquisition matrix 256 × 160 pixels, 5-mm section thickness with no gap), and DW imaging (single-shot echo-planar, 10,000/114.5, field of view 24 cm, acquisition matrix 128 × 128 pixels, 7-mm section thickness with 2-mm gap, diffusion gradient approximately 0 and 1000 cm^2/s, acquired in three orthogonal directions). Intravenous contrast material for T1-weighted imaging consisted of gadopentetate dimeglumine (Magnevist; Berlex Laboratories, Wayne, NJ).

Calculation of ADC maps was based on the following equation:

$$\ln S(G) = \ln S(0) - 2[\gamma^2 \times G^2 \times \delta^2 \times (\Delta - \delta/3)] \times ADC,$$

where G represents the amplitude of the pulsed diffusion gradient, γ the gyromagnetic ratio, Δ the interval between, and δ the duration of the diffusion gradients. S(G) is the signal intensity with diffusion gradient, S (0) the signal intensity without diffusion gradient. ADC maps were generated with software that was supplied by the manufacturer of the MR system.

Registration and Data Analysis

The calculated ADC maps were analyzed by using image processing software (Scion Image, NIH Image; Scion Corporation, www.scioncorp.com/index.htm). Regions of interest (ROIs) were drawn manually onto the obtained ADC maps in the area corresponding to the enhancing region on T1-weighted images. ROIs were shaped to the contour of enhancement and were placed centrally within the solid-enhancing portion of the lesion. Additional ROIs were placed in areas corresponding to T2 prolongation on FLAIR images outside the area of enhancing tissue. For normalization, in each patient, same-size ROIs were also drawn in the matching region of the contralateral hemisphere. The normalization procedure has been used in a recently published study comparing primary meningiomas and high-grade gliomas by using DW imaging and the calculated mean ADC and ADC ratio to determine cellularity in these tumor entities (13). When drawing the matching regions, enhancement in two patients occurred in areas including both white and gray matter of the brain. One patient exhibited enhancement in an area at a level between the basal ganglia and white matter. Another patient's corresponding ROI was found to be located in an area of T2 prolongation according to FLAIR images. ROIs of these patients were additionally adjusted to be located solely in the white matter or outside the T2 prolongation, in a comparable structure. Apart from two patients in whom enhancement was clearly detected only in the cerebral peduncle and the basal ganglia, contralateral ROIs in all other patients were drawn into white matter. To assess the influence of ROI location on ADC assessment in normal parts of the brain, mean ADCs were measured at equivalent sites in both hemispheres in a subset of the nine randomly chosen patients (30 total sites).

For normalizing ADC levels, an ADC_E ratio was calculated as the quotient of the mean ADC values of the enhancing region and the matching structure in the contralateral hemisphere, ADC_{T2} ratio was the quotient of the mean ADC values in T2 prolongation and the contralateral hemisphere, and $ADC_{E/T2}$ ratio was the quotient of mean ADC levels in the enhancing lesion and mean ADC in T2 prolongation. Differences between the ADC of the enhancing lesion and matching contralateral hemisphere and differences between the ADC of T2 prolongation and matching contralateral hemisphere were censored ADC $diff_E$ and ADC $diff_{T2}$, respectively.

Recurrence and nonrecurrence groups were compared by using unpaired *t* test and Mann-Whitney *U* test for mean ADC, mean ADC ratios (ADC_E ratio, ADC_{T2} ratio, $ADC_{E/T2}$ ratio), ADC differences (ADC $diff_E$, ADC $diff_{T2}$), and logarithms of ADC $diff_E$. Paired *t* test was applied for hemisphere comparison outside the brain volume affected by treatment. The level of significance was set at $P < .05$.

Results

Enhancing lesions on T1-weighted images manifested as areas of high mean ADC values compared with mean ADCs of unaffected white matter, surrounding T2 prolongation as hyperintense to white matter on FLAIR images and areas of high mean ADC values compared with mean ADCs of unaffected white matter. All enhancing lesions and areas of T2 prolongation occurred in the radiation target volume of the primary site. Representative T1-weighted, FLAIR, DW images, and ADC maps are shown in Figs 1–3.

In areas separate from abnormal enhancement, outside the T2 prolongation, as well as outside the radiation therapy target volume, diffusion coefficients of the hemispheres were compared. By using 30 different ROIs in nine randomly chosen data sets including patients of both groups, no significant differences between mean ADCs of normal-appearing areas in the hemisphere containing tumor and the contralateral hemisphere of the brain were observed, resulting in a mean ADC ratio of 1.00 ± 0.02 (mean ± SD).

All grade IV tumors were found in the recurrence group, whereas grade III anaplastic tumors were found in both the recurrence and the nonrecurrence groups. Statistical analysis was performed for all tumors in the recurrence group to evaluate for potential bias due to different tumor grades. No significant difference was noted between the mean ADC values of patients with glioblastoma multiforme (grade IV, n = 8) and patients with grade III anaplastic tumors (n = 4). Mean ADC values were $1.20 \pm 0.14 \times 10^{-3}$ mm/s^2 (mean ± SD) for the glioblastoma group and $1.13 \pm 0.13 \times 10^{-3}$ mm/s^2 for the anaplastic glioma group. Mean ADC values and calculated ratios for all 18 patients are listed individually in Table 3 on the Journal's Web site.

The recurrence group showed statistically significant lower mean ADC levels ($1.18 \pm 0.13 \times 10^{-3}$ mm/s^2, mean ± SD) compared with the nonrecurrence group ($1.40 \pm 0.17 \times 10^{-3}$ mm/s^2). The difference reached statistical significance at $P < .006$. Mean ADC values ranged from 0.96 to 1.48×10^{-3} mm/s^2 in the recurrence group, and from 1.11 to 1.55×10^{-3} mm/s^2 in the nonrecurrence group. Figure 4 shows a box and whiskers plot of the mean ADC values. Despite its statistical significance, this plot reveals a relatively broad range of overlapping values in ADC measurements.

We subsequently compared the tumor ADC measurements of a particular patient with ADC measurements of that individual's normal brain (ie, we attempted to obtain intrapersonal data normalization by creating the ratio of ADCs of the enhancing lesion to ADCs of the contralateral, normal, nonenhancing brain parenchyma [ADC_E ratio]). The ratio of the ADC in the enhancing lesion to the contralateral ADC was significantly lower in the recurrence group (1.43 ± 0.11, mean ± SD) compared with that in the nonrecurrence group (1.82 ± 0.07). Significance levels at $P < .001$ were obtained. To normalize in all patients with the matching region within the same anatomic structure, we adjusted ROIs to be located solely in the white matter, outside the cerebral cortex and outside T2 prolongation. Results are shown for ratios after the ROI adjustments. Statistical analysis was performed before and after these ROI adjustments. Adjustments of ROI location into the white

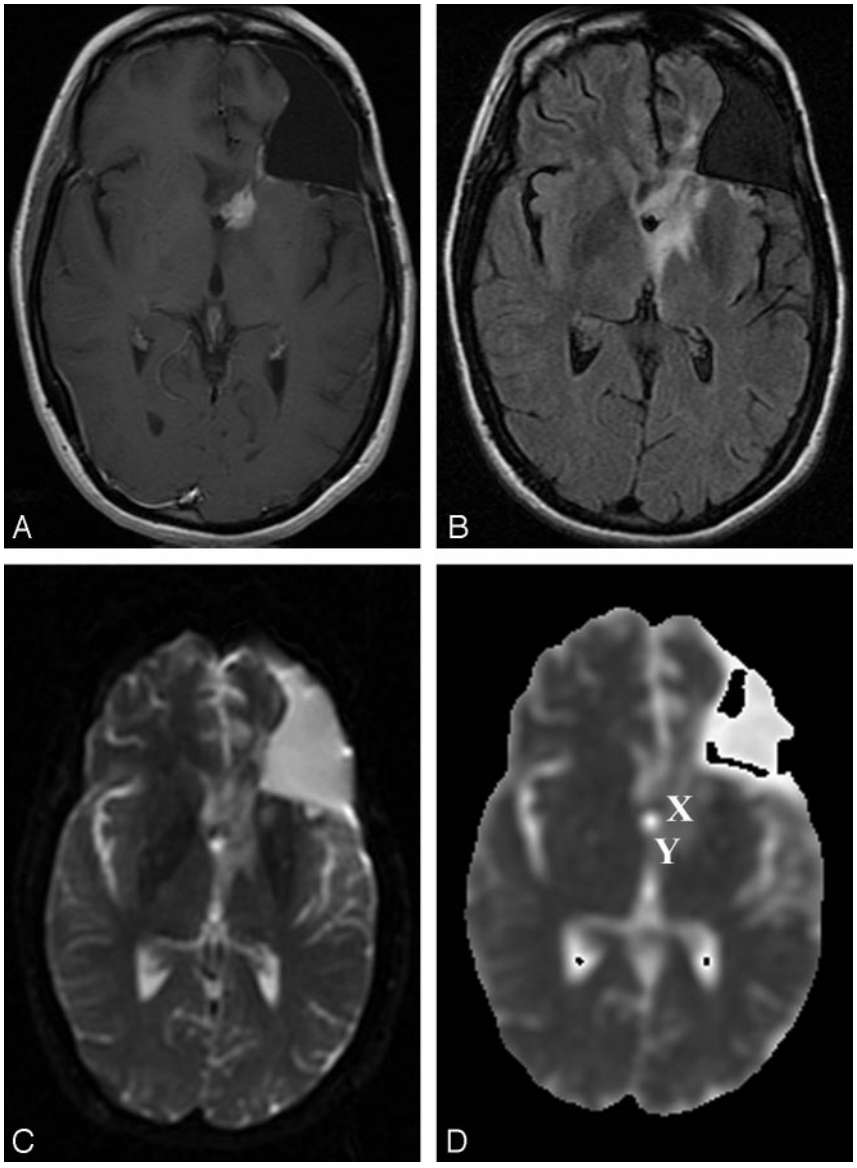

FIG 1. Patient 16 (nonrecurrence group).

A–C, Gadolinium-enhanced T1-weighted (400/14) (*A*), FLAIR (10,002/175/2200) (*B*), and DW echo-planar (10000/114.5, b = 1000 s/mm^2) (*C*) representative axial MR images obtained at follow-up after radiation therapy show a small periventricular enhancing lesion in the left frontal lobe, with a surrounding area of T2 prolongation on the FLAIR image consistent with perifocal edema. Postsurgical changes include an area of prior resection of the primary neoplasm (anaplastic astrocytoma) in the left frontal lobe. Enhancement resolved after hyperbaric oxygen therapy.

D, ADC map from the DW image (b = 0, 1000 S/mm^2). This patient from the nonrecurrence group exhibited a mean ADC in the enhancing lesion of 1.33 $\times$ 10^{-3} mm/s^2, a mean ADC in T2 prolongation of 0.91 $\times$ 10^{-3} mm/s^2, and a normalized ADC ratio of the enhancing region of 1.87. *X* indicates ROI of the enhancing lesion; *Y*, ROI in T2 prolongation.

matter did not change the significance level. A box and whiskers plot illustrating this result is shown in Fig 5.

Mean difference of ADC values between the enhancing lesion and the matching contralateral ROI (ADC diff$_E$) also reached a high significance level ($P < .001$). Mean difference for the recurrence group was recorded as 0.36 $\pm$ 0.11 $\times$ 10^{-3} mm/s^2 (mean $\pm$ SD) and 0.63 $\pm$ 0.10 $\times$ 10^{-3} mm/s^2 for the nonrecurrence group. In addition, we compared the logarithms of the differences between the enhancing lesion and the matching contralateral ROI, which also revealed a significance level of $P < .001$.

Mean ADC in surrounding areas of T2 prolongation was observed as 1.52 $\pm$ 0.14 $\times$ 10^{-3} mm/s^2 (mean $\pm$ SD) in the recurrence group and 1.25 $\pm$ 0.37 $\times$ 10^{-3} mm/s^2 in the nonrecurrence group. Mean ADC in areas of T2 prolongation differed significantly from the mean ADC in normal brain ($P < .001$ and $P = .01$ for the respective groups). We also compared the mean ADC of the enhancing lesion in the recurrence group with the mean ADC in T2 prolongation, which yielded significantly higher ($P < .001$) mean ADC levels in the T2 prolongation. The same comparison of the values in the nonrecurrence group revealed no statistical difference. After calculation of the quotient of mean ADC levels in the enhancing lesion and mean ADC in T2 prolongation (ADC $_{E/T2}$ ratio), a statistical difference between the groups was observed, with a higher mean quotient in the nonrecurrence group (1.16 $\pm$ 0.32, mean $\pm$ SD) compared with that in the recurrence group (0.78 $\pm$ 0.11; $P < .004$).

The ratio of the ADC in T2 prolongation to the contralateral hemisphere (ADC$_{T2}$ ratio) and the difference in ADC between these regions (ADC diff$_{T2}$) could not be used to differentiate the groups.

Statistical analysis was also performed after correction for tumor grade to compare only tumors with WHO grade III in follow-up after therapy. Despite the relatively small sample number, differences between the groups (recurrence, n = 4; nonrecurrence, n = 6) continued to be present for mean ADC values

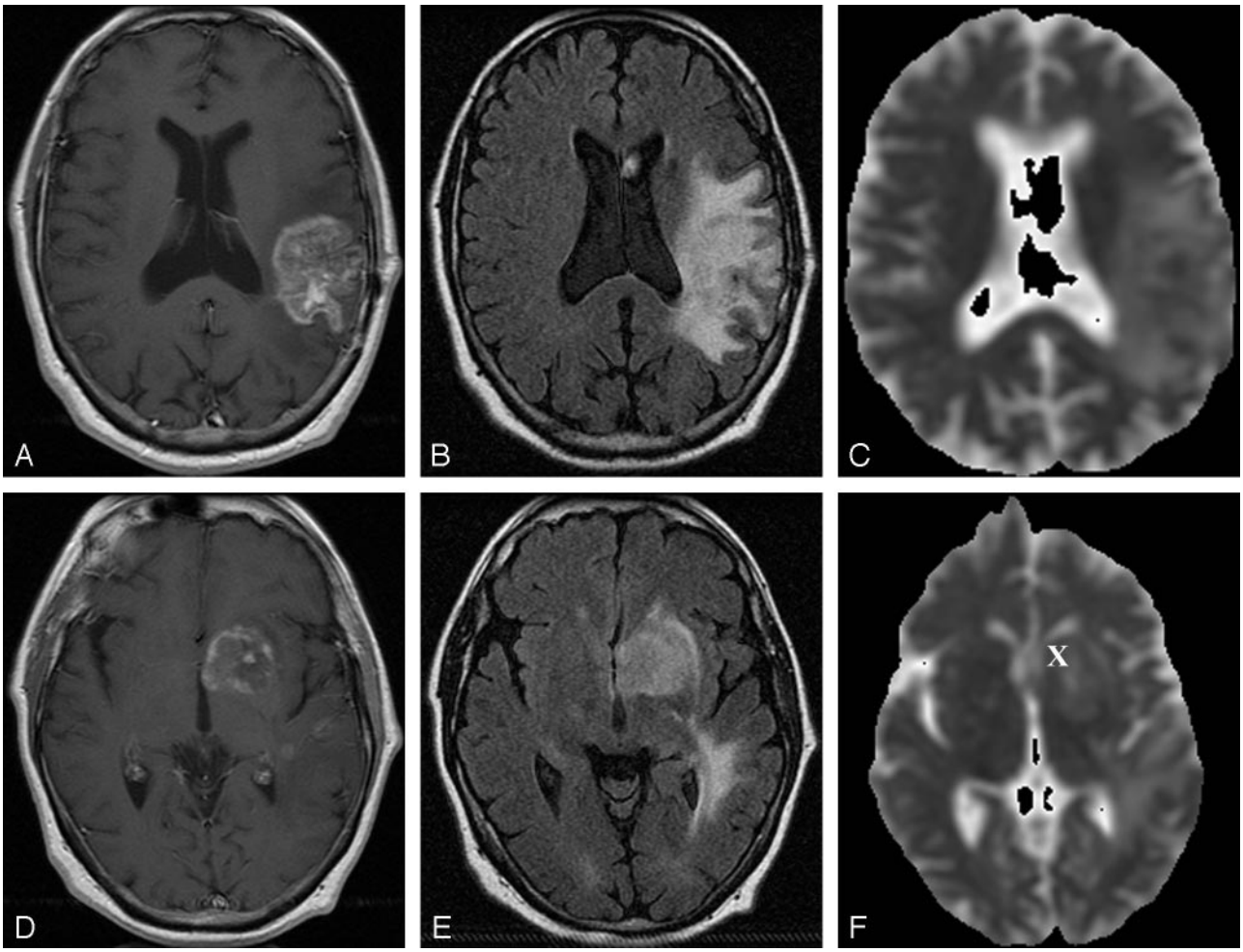

FIG 2. Representative follow-up axial MR images after combined therapy for glioblastoma multiforme in patient 8 (recurrence group).

A–C, Gadolinium-enhanced T1-weighted MR image (400/14) (*A*), FLAIR MR image (10,002/175/22000) (*B*), and ADC map from DW image (b = 0, 1000 s/mm^2) (*C*) obtained at 7-month follow-up after radiation treatment show a left parietotemporal mass with surrounding T2 prolongation.

D–F, Gadolinium-enhanced T1-weighted MR image (400/14) (*D*), FLAIR MR image (10,002/175/22000 (*E*), and ADC map from DW image (b = 0, 1000 s/mm^2) (*F*) show a new focus of enhancement in the left basal ganglia at 7-month follow-up after radiation treatment. Further follow-up imaging (not shown) revealed marked progression of enhancement and T2 prolongation. Patient had progressive functional deterioration in clinical course. This patient from the recurrence group exhibited a mean ADC in the enhancing lesion of 1.13×10^{-3} mm/s^2, a mean ADC in T2 prolongation of 1.64×10^{-3} mm/s^2, and a normalized ADC ratio of the enhancing region of 1.35. *X* indicates ROI of the enhancing lesion. ROI in T2 prolongation was drawn in a different section.

as well as for mean ADC ratio. The differences reached statistical significance with $P < .03$ and $P < .001$, respectively. Figure 6 shows the histologic specimens of the recurrent neoplasm in patient 6 and treatment effects in patient 13. The recurrent lesion, stained with hematoxylin-eosin, was a pleomorphic, hypercellular astrocytic neoplasm with areas of tumor necrosis and prominent endothelial proliferation. The biopsy of the lesion in the patient in the nonrecurrence group showed reactive gliosis and radiation changes with necrosis of nonneoplastic brain.

Discussion

Classifying newly manifested, contrast-enhancing lesions in the follow-up of treated high-grade gliomas with the correct diagnosis is one of the key goals in neuro-oncologic imaging. Therapeutic approach depends on this correct classification, and thus, the decision about additional invasive (biopsy, repeat resection) and noninvasive (radiosurgery, chemotherapy) measures, to obtain a definite diagnosis and increase survival of the patient. Owing to shared imaging characteristics, however, recurrent or progressive glial neoplasm and radiation-induced brain injury are difficult to distinguish. These shared characteristics include proximity to the original tumor site; areas of T2 prolongation that may consist of varying degrees of vasogenic edema, gliosis, and neoplasm; enhancement after the administration of gadopentetate dimeglumine; and varying degrees of mass effect. Areas of abnormal enhancement are considered particularly worrisome for recurrence of aggressive neoplasm. However, this finding reflects only breakdown of the blood-brain barrier, a process that may result from either radiation- and chemotherapy-induced en-

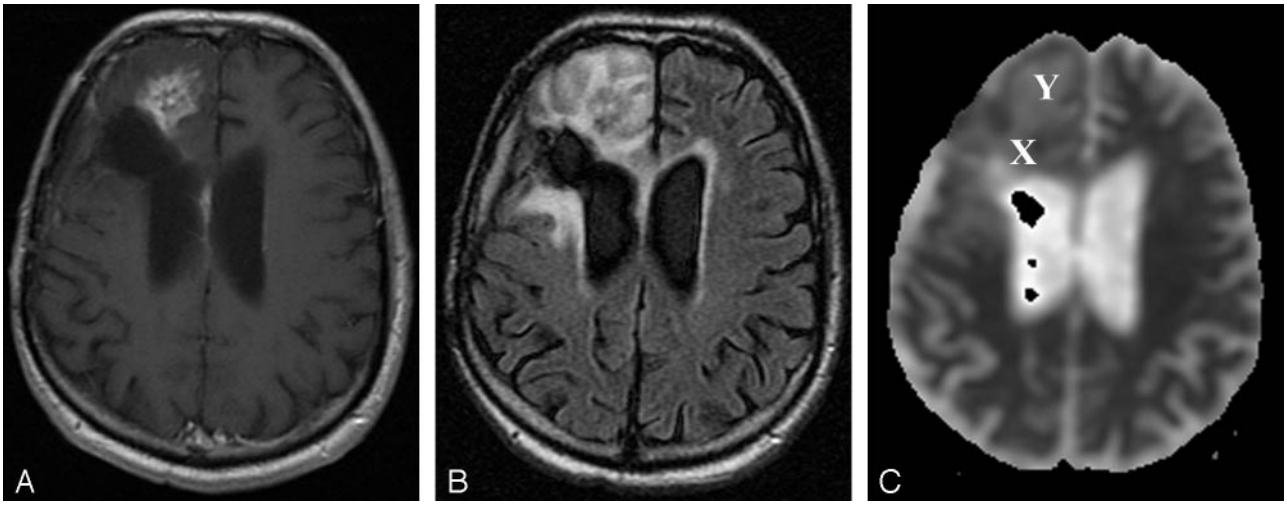

FIG 3. Patient 12 (recurrence group).

A and *B*, Gadolinium-enhanced T1-weighted (400/14) (*A*) and FLAIR (10,002/175/2200) (*B*) representative axial MR images obtained at follow-up show a focus of enhancement close to the resection site (resection of an anaplastic astrocytoma) in the right frontal lobe, with surrounding T2 prolongation. Marked progression of enhancement and perifocal edema were noted on further follow-up images (not shown). Patient had progressive functional deterioration in clinical course, and chemotherapy was restarted.

C, ADC map from DW image (b = 0, 1000 s/mm^2). This patient from the recurrence group exhibited a mean ADC in the enhancing lesion of 1.26×10^{-3} mm/s^2, a mean ADC in T2 prolongation of 1.51×10^{-3} mm/s^2, and a normalized ADC ratio of the enhancing region of 1.62. *X* indicates ROI of the enhancing lesion; *Y*, ROI in T2 prolongation.

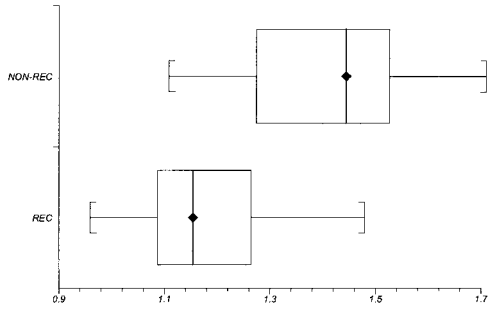

FIG 4. Box and whisker plot compares mean ADC values between the recurrence (*REC*) and nonrecurrence (*NON-REC*) groups. Brackets indicate the range of data; boxes represent the distance between the first and third quartiles, with the median between them marked with a diamond.

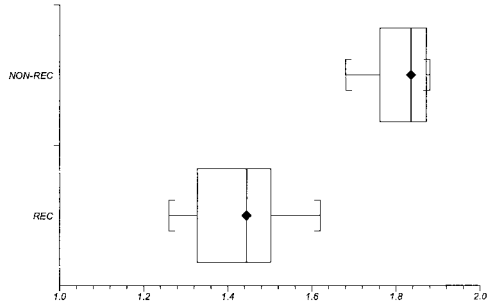

FIG 5. Box and whisker plot compares ADC ratios between the recurrence (*REC*) and nonrecurrence (*NON-REC*) groups. Brackets indicate the range of data; boxes represent the distance between the first and third quartiles, with the median between them marked with a diamond.

dothelial damage of cerebral vessels or loss of adequate tissue perfusion within aggressive neoplasm. The problem is made more complex by the frequent coexistence of recurrent neoplasm and necrosis (5).

In our clinical practice, we have used several imaging modalities in the follow-up of patients treated with radiation and chemotherapy for malignant gliomas. Despite these investigations, biopsy is often deemed necessary, and the results of pathologic examination run counter to the diagnosis suggested by the imaging tests. Other imaging techniques have been assessed for their ablilty to differentiate glial neoplasm and nonneoplastic tissue necrosis. These include dynamic susceptibility contrast-enhanced MR imaging (DSC-MR imaging), MR spectroscopy, PET, and SPECT.

DSC-MR imaging can be useful in the differentiation of the two entities, characterizing tumor recurrence by estimating regional cerebral blood volume, which reflects underlying microvasculature and angiogenesis (4, 14). However, the technique and analysis of the images are difficult, with the marked heterogeneity of flow and the rapid leakage of contrast material across the blood-brain barrier presenting technical obstacles. Further, early studies suggest that many cases will have an indeterminate result (14).

MR spectroscopy has been used to overcome the limited capability of contrast-enhanced MR imaging, by enabling detection of altered levels of biochemical tissue compounds. One study that used retrospective classification of cases by choline-creatinine and choline–*N*-acetylaspartate ratios, achieved correct classification in 82% of cases (15). Results of correlating changes in choline peak with recurrence or radiation-induced brain damage differed (16–18). Multivoxel MR spectroscopy or MR spectroscopic imaging techniques are particularly promising given the spatial complexity of many lesions. However, published data at this time are limited, and no other large series has been published. Furthermore, MR spectroscopy is technically demanding, and in our experience inde-

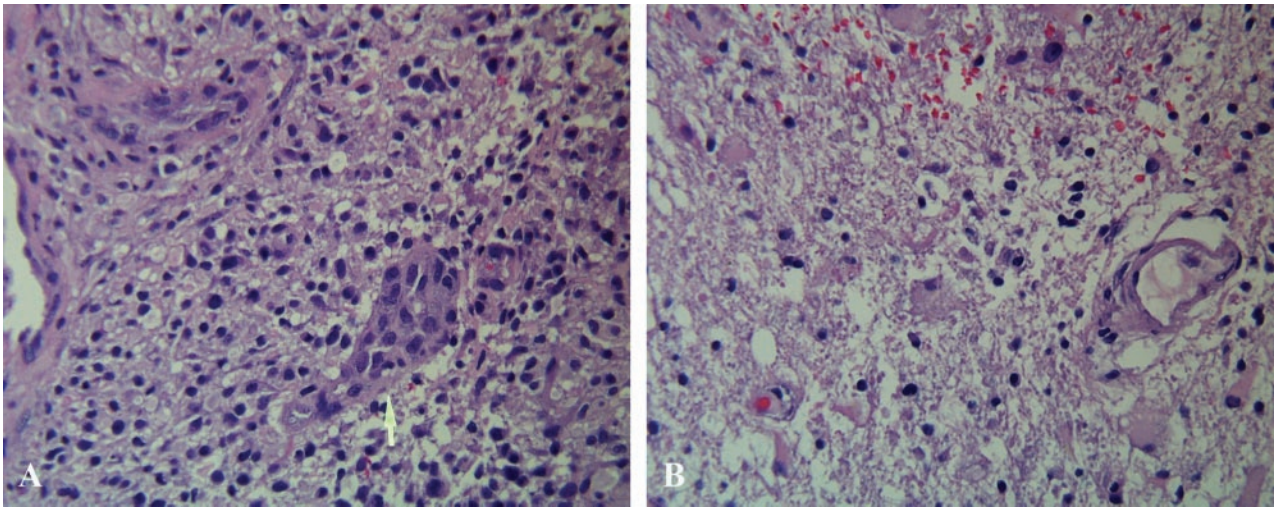

FIG 6.
A, Recurrent neoplasm in patient 6. Photomicrograph (hematoxylin-eosin stain; original magnification, X120) shows the lesion was a pleomorphic, hypercellular astrocytic neoplasm (*arrow*) with areas of tumor necrosis and prominent endothelial proliferation.
B, Histology of treatment effects in patient 13. Photomicrograph (Hematoxylin-eosin stain; original magnification, X120) of biopsy specimen in this patient from the nonrecurrence group shows reactive gliosis and radiation changes, with necrosis of nonneoplastic brain.

terminate metabolite ratios are obtained in many cases. PET and SPECT techniques are also currently in use. Measuring the metabolic state of the tumor, FDG PET and ^{11}C-methionine PET sensitivities and specificities are reported as 75–86% and 22–94%, respectively (2, 19, 20), and the sensitivity of ^{201}Tl SPECT was 92% (21). Comparisons between PET and SPECT revealed different results in terms of their capability to resolve radiation necrosis versus tumor progression (22–24). PET scanners and cyclotrons are still not widely available, and both modalities are considerably limited by a low spatial resolution.

The present study examines the use of DW imaging for differentiation between tumor recurrence and treatment-induced effects. DW imaging uses strong magnetic field gradients to make the MR imaging signal intensity sensitive to the molecular motion of water. The information provided reflects the viability and structure of tissue on a cellular level. DW imaging has proved clinically useful in the evaluation of cerebral ischemia, infection, and some tumors (25–27). The ability of DW imaging to probe the intracellular milieu led to our hypothesis that DW imaging could distinguish neoplasm from nonneoplastic tissue necrosis. Results of previous studies in which authors assessed glial tumors with DW imaging suggested different ADC values due to different tumor grades (11). However, none investigated the ability of DW imaging to discriminate recurrent tumor and treatment-induced necrosis. In contrast to our study, some authors investigated DW imaging in untreated neoplasms; thus, ADCs as well as ADC ratios are not suitable for direct comparison. To eliminate possible bias due to varying ADC in tumors with different tumor grades of the primary neoplasm, the present study was designed to measure ADC in enhancement after therapy in a rather homogeneous group of high-grade gliomas treated with comparable high radiation doses. The absolute ADC values in the recurrence group are similar to those of previous studies. The previously reported values vary from 1.1 to 1.37 $\times$ 10^{-3} mm/s^2 for high-grade glial neoplasms (6, 11, 12), including the only study characterizing enhancing tissue in primary as well as in residual or recurrent high-grade gliomas treated with radiation therapy (7). The only study using the ADC ratio as a quantitative parameter in high-grade gliomas calculated a mean ADC ratio of 1.68 $\pm$ 0.48 (13).

ADC values of biologic tissue are determined by many factors. The motion of the protons is restricted by such barriers as membranes, organelles, cytoskeleton, and macromolecules inside different tissue compartments. Also, the size and number of mobile protons in these compartments can vary. For example, a shift of water from the extracellular to intracellular spaces is responsible for a large part of the decreased ADC values observed in acute cerebral ischemia (26). For brain tumors, cellularity likely plays an important role. With higher diffusivity found in the extracellular volume, the increase of intracellular space due to highly cellular tissue is coupled with a decrease of the ADC. Higher cellularity in recurrent neoplasm would contribute to the lower ADC values (9, 13). Thus, growth of recurrent, viable tumor cells determining in part the tissue ADC within the enhancing region in the recurrence group might explain the differences in mean ADC levels between the patient groups in our study. The histologic finding of a hypercellular tumor (grade IV) in the specimen (Fig 6A) from a patient in the recurrence group could support this hypothesis. Cellularity is only one important factor that might influence the ADC after therapy. The different contributions of other components (eg, necrosis, gliosis, fibrous scar tissue, or granulation tissue) to the ADC of brain parenchyma after therapy have not been determined so far in absolute values. For that reason, we can only speculate about higher

mean ADC values in enhancing tissue that are induced by radiation injury because of a different relative fraction and hence influence of these components on mean ADC. However, the direct comparison between the histologic samples of the two groups could again demonstrate the likewise higher influence of cellularity on ADC of the enhancing tissue (Fig 4). Low signal intensities on DW images of temporal lobe necrosis after radiation therapy of nasopharyngeal carcinomas are reported, but we could find only one ADC value (ie, 2.88×10^{-3} mm/s^2) in the literature (10, 28).

The exact mechanisms of radiation injury are still not completely understood. The influence of multiple variables, including total dose of radiation, field and fraction number and size, combined radiation and chemotherapy, and clinical status or age of the patient, on treatment-induced effects of the brain is unknown. In addition, the time of occurrence of immediate and delayed type of reactions varies. With most of our examinations being performed at follow-up in the first year after completed radiation therapy, vascular injury and glial damage are postulated mechanisms for radiation effects at this time (5). This might be the reason why the ADCs in our study did not correspond to those reported for nonenhancing, complete radiation necrosis in the temporal lobe after irradiation for nasopharyngeal carcinoma (28).

The statistical evaluation of our data revealed a significant difference in mean ADCs between the group of patients with treatment effects and the group with tumor recurrence. However, using the ADC ratio substantially improved the differentiation of these two groups in our study. After the normalization procedure mentioned in Methods, a highly significant difference of the normalized mean ADC ratio as well as the mean difference between the contrast-enhancing and the contralateral hemispheres was observed. Although the mean ADCs differed between the groups, the ADC ratio seems to be a better parameter to distinguish the underlying pathologic conditions responsible for the contrast enhancement. Furthermore, the ADC ratio should minimize the differences in absolute ADC that may be obtained with different DW imaging sequences. Our results, while preliminary, suggest that the mean DW imaging ratio of enhancing tissue can be used to distinguish recurrent neoplasm from treatment-related necrosis. Using this parameter, there were no overlapping data between the groups, which resulted in a threshold level for differentiation. Mean ADC ratios higher than 1.62 only occurred in treatment-related necrosis, and mean ADC ratios lower than this threshold only occurred in recurrent neoplasm.

The area of T2 prolongation outside the region of blood-brain barrier breakdown also differed between recurrent neoplasm and treatment-related necrosis. ADCs in peritumoral edema have been reported with values ranging between 1.29 and 1.42×10^{-3} mm/s^2 (7, 9). No data about ADC values in this region in follow-up of treated high-grade gliomas could be found in the literature. Calculating the ADC ratio between the enhancing region and the surrounding area of T2 prolongation (ADC ratio$_{E/T2}$) yielded another statistically significant parameter that could be used for differentiation.

Noteworthy limitations of our study were the small number of patients, the lack of histologic confirmation in all cases (although one can argue that the clinical course in follow-up is as reliable an indicator as histologic examination, considering the difficulties to differentiate histologically between posttreatment effects, recurrent neoplasm, and tissue in which both are present in varying proportions), and technical difficulties in correlating the abnormal enhancing regions with the corresponding region in the ADC maps. Although histologic confirmation in all patients may be desirable, it is not always clinically practicable. In an approach similar to that of other published studies (15), we used the clinical course in follow-up as a surrogate indicator of histology (mean follow-up for patients without histologic confirmation in the nonrecurrence group was 15.5 months).

DW imaging has many practical advantages that make its use an attractive alternative to other imaging modalities. It is part of standard neuroimaging at many institutions and incurs no additional costs. With use of fast imaging sequences (echo planar imaging) and with ADC calculating software integrated in the workstation, DW imaging is not time-consuming. Spatial resolution is sufficient to demarcate the lesions and is superior to that of PET and SPECT.

Conclusion

The results of this preliminary study suggest that assessment of the ADC in enhancing lesions in the follow-up of treatment for high-grade glial tumors enables differentiation of recurrent lesions from therapy-induced effects. Assessment of ADC in surrounding tissues may further improve this ability. To our knowledge, the present study is the first in which mean ADC values and ADC ratios of these tissue morphologic features were quantitatively compared. DW imaging may become an important imaging option for follow-up of high-grade gliomas.

References

1. Samnick S, Bader JB, Hellwig D, et al. **Clinical value of iodine-123-alpha-methyl-L-tyrosine single-photon emission tomography in the differential diagnosis of recurrent brain tumor in patients pretreated for glioma at follow-up.** *J Clin Oncol* 2002;20:396–404
2. Langleben DD, Segall GM. **PET in differentiation of recurrent brain tumor from radiation injury.** *J Nucl Med* 2000;41:1861–1867
3. Schlemmer HP, Bachert P, Henze M, et al. **Differentiation of radiation necrosis from tumor progression using proton magnetic resonance spectroscopy.** *Neuroradiology* 2002;44:216–222
4. Sugahara T, Korogi Y, Tomiguchi S, et al. **Posttherapeutic intraaxial brain tumor: the value of perfusion-sensitive contrast-enhanced MR imaging for differentiating tumor recurrence from nonneoplastic contrast-enhancing tissue.** *AJNR Am J Neuroradiology* 2000;21:901–909
5. Kumar AJ, Leeds NE, Fuller GN, et al. **Malignant gliomas: MR imaging spectrum of radiation therapy– and chemotherapy-induced necrosis of the brain after treatment.** *Radiology* 2000;217:377–384
6. Brunberg JA, Chenevert TL, McKeever PE, et al. **In vivo MR determination of water diffusion coefficients and diffusion aniso-**

tropy: correlation with structural alteration in gliomas of the cerebral hemispheres. *AJNR Am J Neuroradiol* 1995;16:361–371
7. Castillo M, Smith JK, Kwock L, Wilber K. **Apparent diffusion coefficients in the evaluation of high-grade cerebral gliomas.** *AJNR Am J Neuroradiol* 2001;22:60–64
8. Lam WW, Poon WS, Metreweli C. **Diffusion MR imaging in glioma: does it have any role in the pre-operation determination of grading of glioma?** *Clin Radiol* 2002;57:219–225
9. Kono K, Inoue Y, Nakayama K, et al. **The role of diffusion-weighted imaging in patients with brain tumors.** *AJNR Am J Neuroradiol* 2001;22:1081–1088
10. Tsui EY, Chan JH, Ramsey RG, et al. **Late temporal lobe necrosis in patients with nasopharyngeal carcinoma: evaluation with combined multi-section diffusion weighted and perfusion weighted MR imaging.** *Eur J Radiol* 2001;39:133–138
11. Sugahara T, Korogi Y, Kochi M, et al. **Usefulness of diffusion-weighted imaging with echo-planar technique in the evaluation of cellularity in gliomas,** *J Magn Reson Imaging* 1999;9:53–60
12. Krabbe K, Gideon P, Wagn P, Hansen U, Thomsen C, Madsen F. **MR diffusion imaging of human intracranial tumours.** *Neuroradiology* 1997;39:483–489
13. Guo AC, Cummings TJ, Dash RC, Provenzale JM. **Lymphomas and high-grade astrocytomas: comparison of water diffusibility and histologic characteristics.** *Radiology* 2002;224:177–183
14. Cha S, Knopp EA, Johnson G, et al. **Dynamic contrast-enhanced T2-weighted MR imaging of recurrent malignant gliomas treated with thalidomide and carboplatin.** *AJNR Am J Neuroradiol* 2000; 21:881–890
15. Schlemmer HP, Bachert P, Herfarth KK, Zuna I, Debus J, van Kaick G. **Proton MR spectroscopic evaluation of suspicious brain lesions after stereotactic radiotherapy.** *AJNR Am J Neuroradiol* 2001;22:1316–1324
16. Graves EE, Nelson SJ, Vigneron DB, et al. **Serial proton MR spectroscopic imaging of recurrent malignant gliomas after gamma knife radiosurgery.** *AJNR Am J Neuroradiol* 2001;22:613–624
17. Traber F, Block W, Flacke S, et al. **1H-MR spectroscopy of brain tumors in the course of radiation therapy: use of fast spectroscopic imaging and single-voxel spectroscopy for diagnosing recurrence.** *Fortschr Röntgenstr* 2002;174:33–42
18. Chong VF, Rumpel H, Fan YF, Mukherji SK. **Temporal lobe changes following radiation therapy: imaging and proton MR spectroscopic findings.** *Eur Radiol* 2001;11:317–324
19. Chao ST, Suh JH, Raja S, Lee SY, Barnett G. **The sensitivity and specificity of FDG PET in distinguishing recurrent brain tumor from radionecrosis in patients treated with stereotactic radiosurgery.** *Int J Cancer* 2001;96:191–197
20. Chung JK, Kim YK, Kim SK, et al. **Usefulness of 11C-methionine PET in the evaluation of brain lesions that are hypo- or isometabolic on 18F-FDG PET.** *Eur J Nucl Med Mol Imaging* 2002;29:176–182
21. Stokkel M, Stevens H, Taphoom M, Van Rijk PP. **Differentiation between recurrent brain tumor and post-radiation necrosis: the value of 201T1 SPET versus 18F-FDG PET using dual headed coincidence camera—a pilot study.** *Nucl Med Commun* 1999;20: 411–417
22. Weber W, Bartenstein P, Gross MW, et al. **Fluorine-18-FDG PET and iodine 123-IMT-SPECT in the evaluation of brain tumors.** *J Nucl Med* 1997;38:802–808
23. Sonoda Y, Kumabe T, Takahashi T, Shirane R, Yoshimoto T. **Clinical usefulness of 11C-MET PET and 201T1 SPECT for differentiation of recurrent glioma from radiation necrosis.** *Neurol Med Chir* 1998;38:342–347
24. Thompson TP, Lunsford LD, Kondziolka D. **Distinguishing recurrent tumor and radiation necrosis with positron emission tomography versus stereotactic biopsy.** *Stereotact Funct Neurosurg* 1999; 73:9–14
25. Mullins ME, Schaefer PW, Sorensen AG, et al. **CT and conventional and diffusion-weighted MR imaging in acute stroke: study in 691 patients at presentation to the emergency department.** *Radiology* 2002;224:353–360
26. Schaefer PW, Ozsunar Y, He J, et al. **Assessing tissue viability with MR diffusion and perfusion imaging.** *AJNR Am J Neuroradiol* 2003;24:436–443
27. Stadnik TW, Chaskis C, Michotte A, et al. **Diffusion-weighted MR imaging of intracerebral masses: comparison with conventional MR imaging and histologic findings.** *AJNR Am J Neuroradiol* 2001; 22:969–976
28. Park SH, Chang KH, Song IC, Kim YJ, Kim SH, Han MH. **Diffusion-weighted MRI in cystic and necrotic intracranial lesions.** *Neuroradiology* 2000;42:716–721